Chiang Mai J. Sci. 2010; 37(2) : 269-281
www.science.cmu.ac.th/journal-science/josci.html
Contributed Paper

Age Hardening and Precipitation Behavior of an Experimental Cast Al-Mg-Si Alloy Treated by T6 and T6I6 Heat Treatments

Suttawan Imurai [a], Julatep Kajornchaiyakul [b], Chachana Thanachayanont [b], John T.H. Pearce [b] and Torranin Chairuangsri*[a]

[a] Department of Industrial Chemistry, Faculty of Science, Chiang Mai University, Chiang Mai 50200, Thailand.

[b] National Metal and Materials Technology Center, Bangkok, 10400, Thailand.

*Author for correspondence; e-mail: chato@chiangmai.ac.th

Received: 30 December 2009
Accepted: 26 February 2010

ABSTRACT

An experimental Al-7.32wt%Si-0.3wt%Mg alloy equivalent to cast A356 Al-Mg-Si alloy was studied. Age hardening was performed by two artificial ageing heat treatments, T6 and T6I6. Vickers microhardness was measured within the dendritic regions. It was found that peak ageing was reached after about 24 hours. T6 and T6I6 increased the hardness from the as-cast value by 52 % and 60 %, respectively. The peak hardness achieved *via* T6I6 is approximately 8 % higher than that obtained by T6. Overall microstructure was studied by scanning electron microscopy and energy dispersive x-ray spectrometry. Eutectic constituents were revealed as Si flakes and Fe-bearing intermetallic compounds including π-Chinese script phase ($Al_8Mg_3FeSi_6$) and β(Al_5FeSi). Precipitation behavior was investigated by transmission electron microscopy and the precipitation sequence found was somewhat in agreement with those reported previously for wrought and cast Al-Mg-Si alloys. However, the peak hardness ageing period coincided with the presence of β'' phase or its precursors, not β' phase.

Keywords : Cast Al-Mg-Si Alloy, A356, Age Hardening, Heat Treatment, Precipitation Behavior, Electron Microscopy.

1. INTRODUCTION

Aluminium is increasingly attractive due to its strength and stiffness to weight ratio. Al-Mg-Si alloys are age hardenable and widely used in both cast and wrought forms. Strengthening of Al-Mg-Si alloys is based on a precipitation hardening process. Their importance and significant age-hardening response has provoked numerous studies of precipitation in these alloys.

Wrought Al-Mg-Si alloys of 6xxx series are alternatives to steel for automotive body applications since they show good combination of formability, corrosion resistance and weldability [1]. Due to the complex nature of the precipitation sequence in both wrought and cast alloys together with the difficulties in identification and chemical charaterisation of the fine scale microstructures, there is still

controversy over the exact sequence of struc-tural changes during ageing [2]. For the wrought alloys without excess Si or the so called balanced alloys, it has been reported that the precipitation sequence is independent of the composition [3,4]. A precipitation sequence that is generally accepted is, e.g. [1,5].

SSS $\alpha \rightarrow$ GP zones (spheres or needles) $\rightarrow \beta''$ (needles)$\rightarrow\beta'$ (rods)$\rightarrow\beta$ (plates, Mg_2Si or nonstoichiometric Mg_xSi_y)

SSS denotes "supersaturated solid solution" and GP denotes "Guinier-Preston". Another precipitation sequence with more detail on the earlier stage of clustering and GP-zone formation was proposed [6] as:

SSS $\alpha\rightarrow$ clusters of Si atoms$\rightarrow$ GP-I zones$\rightarrow$GP-II zones or $\beta''\rightarrow\beta'\rightarrow\beta$ (Mg_2Si).

More complicated earlier changes and the formation of an additional phase (B'), together with β', have also been proposed [2] as:

SSS $\alpha \rightarrow$ clusters of Si atoms + clusters of Mg atoms $\rightarrow$ dissolution of Mg clusters $\rightarrow$ formation of (Mg,Si) co-clusters small precipitates of unknown structure or GP zones $\rightarrow \beta'' \rightarrow \beta'$ or $B' \rightarrow \beta$ (Mg_2Si)

It should be noted that B' phase is identical to M phase [7] or Q* phase [8] denoted in some literature. Some wrought aluminium alloys for automobile applications generally contain an excess of Si above that required to form stoichiometric Mg_2Si [4]. The amount of excess Si can be calculated by considering that the Mg:Si weight ratio in Mg_2Si formation is 1.73:1 and assuming that the Fe:Si weight ratio for the formation of Fe-rich particles is 4:1, hence a relation can be written as follows [4].

$$\text{Excess Si} = (\text{wt\% Si in alloy}) - \left[\left(\frac{\text{wt\% Mg in alloy}}{1.73}\right) + \left(\frac{\text{wt\% Fe in alloy}}{4}\right)\right]$$

The precipitation sequence for Al-Mg-Si alloys containing excess Si was proposed [9] as:

SSS $\alpha\rightarrow$(Mg+Si) co-clusters or (platelike/spherical) GP-I$\rightarrow\beta''$ or GP-II (needles) $\rightarrow\beta'$ (rods) + Si + others$\rightarrow\beta$ (Mg_2Si) plates + Si.

It has been suggested that the excess Si does not alter the precipitation sequence, structure and lattice parameters of different metastable precursors, but rather results in modification of the composition and density of particles [2,10,11]. However, excess Si seems to promote formation of additional phases during later stages of aging [2,10,11], but does not contribute significantly to hardening [9]. Cu-containing Al-Mg-Si alloys are another predominant group used for sheet in the automotive industry. Additional quarternary phases are formed as a result of Cu addition. The complex decomposition sequence for Al-Mg-Si-Cu alloys with a balanced Mg to Si ratio is generally considered to be [12]:

SSS $\alpha \rightarrow$ clusters or co-clusters of Mg+Si $\rightarrow$ GP zones $\rightarrow \beta'' \rightarrow \beta' + Q' \rightarrow \beta(Mg_2Si) + Q(Al_4Cu_2Mg_8Si_7)$.

Other precursors of the quarternary Q phase were also reported, denoted as QP and QC [13].

Cast A356 (Al-0.3wt%Mg-7wt%Si) aluminium alloy is commonly used as cylinder head and engine block material [14]. It has widespread applications for structural components in the automotive, aerospace and general engineering industries because of its excellent castability, corrosion resistance and particularly high strength-to-weight ratio in the heat-treated condition [15,16]. However, the use of this cast alloy is still limited in comparison with wrought Al alloys, even though casting is a more economical production method [16]. This is partly because cast Al alloys may contain defects such as porosity, oxides and other inclusions, which significantly affect the mechanical properties of the cast Al components. Cast A357 (Al-0.5wt% Mg-7wt%Si) alloy also possesses excellent castability and good fatigue and corrosion resistance properties. These alloys are normally used in the T6 condition, which involves solution treatment, quenching and artificial aging [17]. The optimum balance of strength and ductility attained after thermal treatment is attributed to the changes in eutectic Si characteristics resulting from the solution treatment and to the formation of non-equilibrium precipitates of β' resulting from the aging treatment [18,19]. The maximum solubility of Si in Al is 0.05 wt% at room temperature and the alloy contains 6.5-7.5 wt% Si, accordingly, any excess Si exists as relatively large (1-10 μm) eutectic Si platelets [19].

From the above review on both wrought and cast Al-Mg-Si alloys, it can be seen that, despite a long-time study, clear understanding of the nature of precipitating phases in Al-Mg-Si alloys has not yet been achieved. Confusion remains regarding (i) initial clustering processes, (ii) structures and compositions of all intermediate precipitates, (iii) consistent evidence over the nature and type of intermediate phases that are formed during the precipitation sequence and (iv) phases giving peak strength reported as β'' for wrought alloys and as β' for cast alloys. Relatively few studies have been performed on cast alloys, especially by electron microscopy. Therefore, a study of precipitation behavior and its relationship to the aged properties of cast Al-Mg-Si alloy are of interest since any change in composition, processing and ageing practices etc. could affect the precipitation hardening behavior. Moreover, Buha et al.[12] recently utilized the T6I6 heat treatment in Al-Mg-Si-Cu (6061) alloy, where T6 indicates the standard T6 treatment and I6 indicates an interruption by secondary ageing at lower temperature (typically between 25-65°C) before resuming the final ageing at the temperature of the initial T6 treatment or at another different elevated temperature. Their results revealed that secondary ageing promoted secondary precipitation of GP zones and consequently a significantly greater number of precursors to the β'' precipitates were produced. Hence, it is also of interest to investigate the effect of the T6I6 treatment on the structure and properties of cast Al-Mg-Si alloy in comparison to that of the T6 treatment.

2. MATERIALS AND METHODS

2.1 Materials

An experimental alloy was prepared by gravity casting at the National Metal and Material Technology Center, Pathumthani, Thailand, to be equivalent to cast A356 Al-Mg-Si alloy The chemical analysis by spark emission spectrometry is given in Table 1.

Table 1. Chemical composition of the experimental cast Al-Mg-Si alloy equivalent to A356.

Elements	Si	Mg	Fe	Cu	Mn	Ti	Zn	Sn	Ni	Al
wt%	7.32	0.3	0.147	< 0.002	0.006	0.127	< 0.001	< 0.003	0.005	bal.

Top view illustration of the tapered-shape casting is given in Figure 1. It was cut by a Labotom-3, Struers cutting machine as specimens with a dimension of approximately 0.9 cm × 0.9 cm × 3.5 cm as marked by dotted lines in Figure 1.

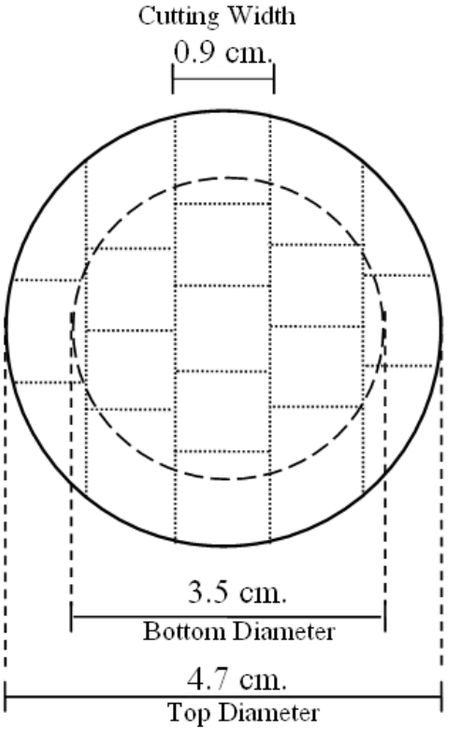

Figure 1. Dimension of the tapered-shape casting before cutting as specimens along dot lines.

2.2 Heat Treatment

Despite the formation of a protective alumina film, specimens were encapsulated in a silica tube under a partial pressure of argon gas before heat treatment to ensure oxidation protection. Solution treatment was performed at 540°C for 4 hours followed by breaking the silica tube under water for quenching. Specimens were left for natural ageing at room temperature in air for 45 weeks. Consequently, artificial ageing was performed using an oil bath. T6 artificial ageing was done at 160°C for 8-500 hours followed by quenching in water. T6I6 artificial ageing was done at 160°C for 20 minutes, interrupted by low temperature ageing at 65°C for 2 weeks, then resumed at 160°C for 8-200 hours followed by quenching in water. Outlines of the T6 and T6I6 heat treatment cycles are given in Figure 2.

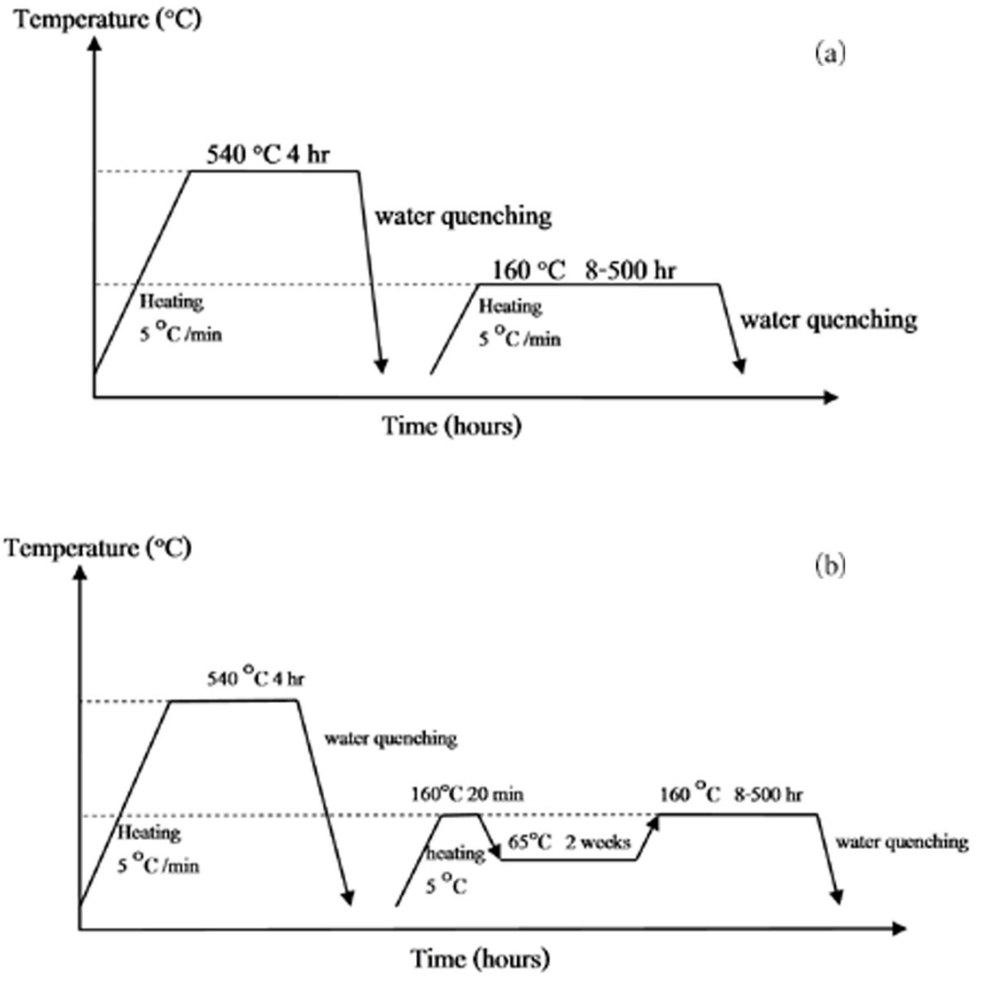

Figure 2. Time schedule of heat treatment: (a) T6 artificial ageing and (b) T6I6 artificial ageing.

2.3 Vickers Microhardness Measurement

Specimens were ground and polished by a normal metallographic procedure. Vickers microhardness measurement was performed in primary α-Al dendrites using a Microscan OD, Galileo tester with 100 gf load for 15 seconds.

2.4 Microstructural Investigation

For scanning electron microscopy, polished specimens were deep-etched using an aqueous solution of 15 wt% cupric chloride for up to 5 seconds. They were rinsed by an aqueous solution of 50 wt% nitric acid to get rid of copper, followed by distilled water and methanol. A JSM 5910LV JEOL scanning electron microscope operated at 15 kV, equipped with Inca, Oxford EDS detector, was used.

For transmission electron microscopy, specimens were cut as 150-200 μm thick by an Accutom-2, Struers, cutting machine, ground to 100-120 μm thick using 1,200 grit silicon carbide paper, and punched as 3-mm

discs. Discs were further ground down to about 80 μm thick before twin-jet electro-polishing on a Tenupol-3, Struers polishing machine using 5 vol% perchloric acid in absolute ethanol as electrolyte. Controlled parameters were 37 V, about 16 mA, and the temperature range of -5 to -15°C. A JEM 2010 JEOL transmission electron microscope, operated at 200 kV, was used to study the specimens.

3. RESULTS AND DISCUSSION

3.1 Vickers Microhardness

Results from Vickers microhardness measurement within the dendritic regions are shown in Figure 3, by comparing the as-cast value to those obtained after T6 or T6I6 ageing treatment. For both T6 and T6I6, the peak ageing was reached after about 24 hours. The peak hardness by T6 was about 92±7 kgf/mm^2, while that by T6I6 is approximately 8 % higher, i.e. about 99±3 kgf/mm^2. The hardness from the as-cast specimen was about 624 kgf/mm^2. Therefore, age hardening by T6 and T6I6 in this experiment increased the hardness by 52 % and 60 %, respectively. It should be noted that rate of decrease from the peak hardness in the over-ageing period was faster in the case of T6I6.

3.2 Microstructural Investigation by SEM and TEM

Figure 4 shows SEM backscattered electron images (BEI) from unetched specimens in as-cast (Figure 4(a)), solution treated (Figure 4(b)) and T6 aged (Figure 4(c)) conditions. The structures in these conditions are comparable, except that some spheroidi-sation of the eutectic silicon occurred after solution and ageing treatment.

Results from SEM-EDS point analyses at positions 1 to 3 across the a-Al dendrite are given in Table 2. In the as-cast condition, segregation of Si to edge of dendrite was observed. On the other hand, Si was distributed uniformly after solution treatment

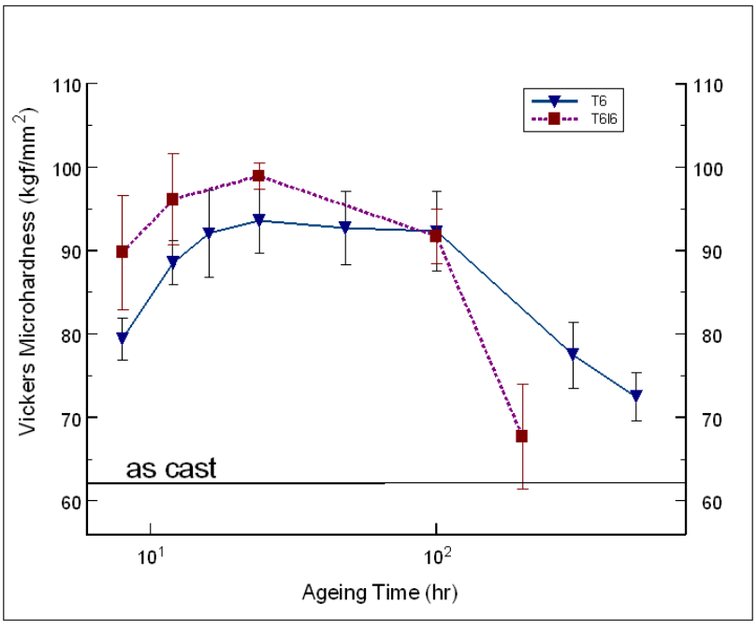

Figure 3. Relationship between Vickers microhardness and the ageing time of the alloy after T6 or T6I6 heat treatment.

confirming the sufficiency of solution treatment temperature and time in this experiment. As expected, SEM-EDS point analysis could not detect any different in Si distribution after ageing treatment.

The eutectic structure contains mainly of

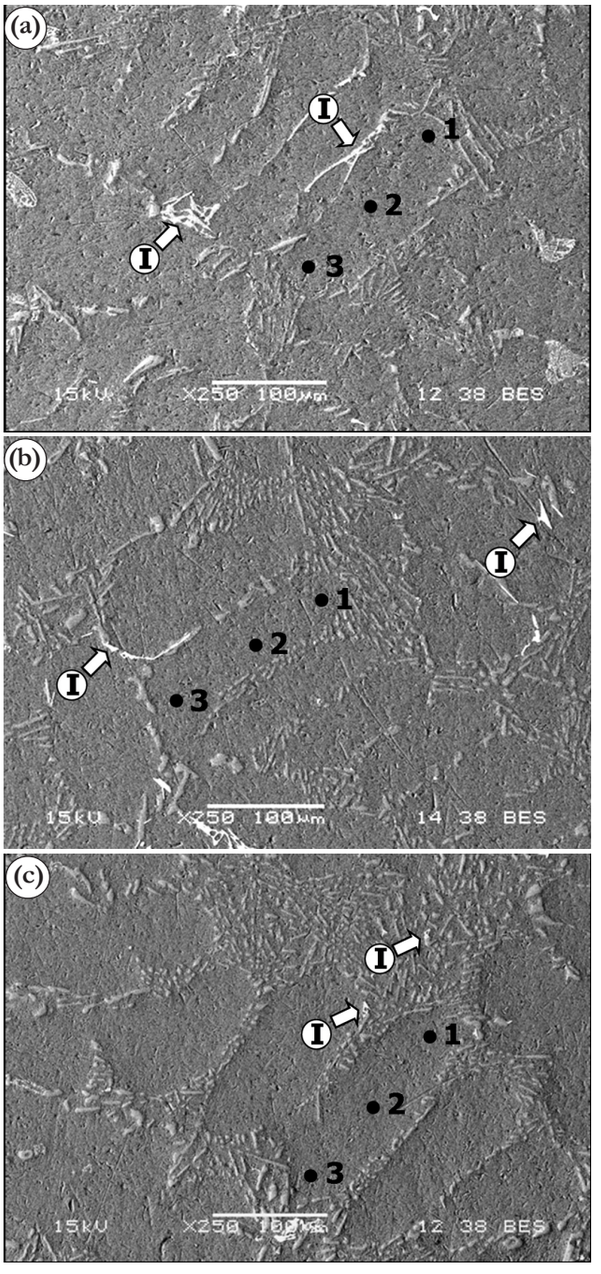

Figure 4. SEM-BEI of unetched specimens in (a) as-cast, (b) solutionised and (c) T6 aged conditions. 'I' marked intermetallic compounds associated with eutectic structure. Numbers 1, 2 and 3 marked the positions at which the EDS point analyses were performed as reported in Table 2.

Table 2. Semi-quantitative SEM-EDS analysis of Si content within a-Al dendrites in Figure 4.

SEM-EDS point analysis positions	Si content (wt%) in α-Al dendrites after different heat-treated conditions		
	as-cast (Figure 4(a))	after solution treatment (Figure 4(b))	after T6 ageing (Figure 4(c))
1	2.15	1.47	1.29
2	0.81	1.52	1.38
3	6.07	1.24	1.38

Si flakes as shown at higher magnification in SEM secondary electron image (SEI), for example in Figure 5. Some iron-containing intermetallic compounds were also found appearing with the brightest contrast in SEM-BEI as marked 'I' in Figure 4. As indicated in Figure 5, one constituent that contains Mg can be p-Chinese script phase ($Al_8Mg_3FeSi_6$) and the other can be β(Al_5FeSi) phase. These microstructural observations are in agreement with previous work [19-23].

Figure 6(a) is a bright-field (BF) TEM micrograph showing the microstructure in an α-Al dendrite after solution treatment. No precipitation was observed in this condition. The inset is a selected area diffraction pattern (SADP) which contains only spots from the α-Al. For the under-ageing T6 period,

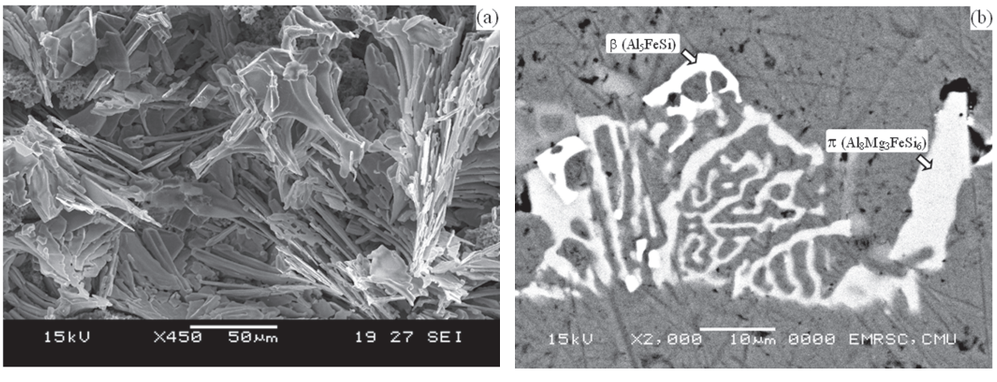

Figure 5. (a) SEM-SEI shows flake-like, eutectic Si in the alloy after deep etching and (b) SEM-BEI shows Fe-bearing intermetallic compounds associated with eutectic structure, identified as π-Chinese script ($Al_8Mg_3FeSi_6$) and β (Al_5FeSi) phases.

apparent spheroidal dark contrast was found with fine size of about 3-5 nm in BF mode (Figure 6(b)). The corresponding SADP in $<001>_{Al}$ shows no separate pattern from this phase nor streaking on the matrix spots (as shown inset). Therefore, it can be isostructural with the Al matrix. By comparing its characteristics with those of phases found in wrought Al-Mg-Si alloys, it is comparable to spheroidal GP zones or so called "GP-I" [1,2,5,6].

At peak T6 ageing, a needle-shaped phase with the needle axis lying along $<001>_{Al}$ was observed in TEM-BF mode. Three orthogonal orientation variances of this phase along $[001]_{Al}$ direction can be seen in Figure

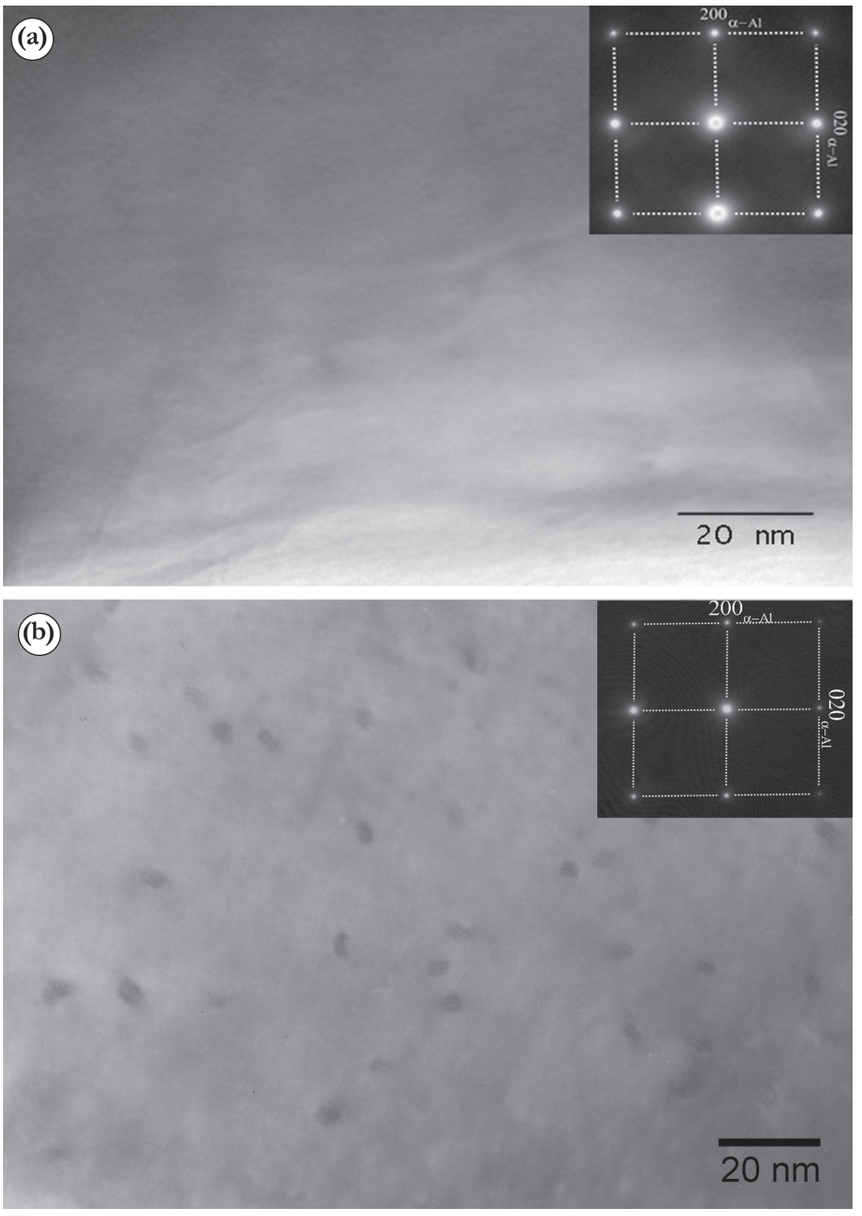

Figure 6. BF-TEM micrographs show the microstructure in the a-Al matrix; (a) after solution treatment and (b) after T6 ageing for 16 hours corresponding to the under-ageing peroid. Corresponding SADPs are given as insets.

7(a). Its length is about 20 nm and apparent cross-sectional diameter is about 2-4 nm. Even though it was noted that streaks on SADP by GP zones as observed e.g. in Al-Cu alloys is unlikely since atomic scattering factors of Al, Si and Mg are all very similar[2], streaking on the Al spots in SADP (Figure 7(b)) was surprisingly observed in this condition in $g<001>_{Al}$ directions as enlarged for example in Figure 7(c). Some characteris-

tics of this phase are partly comparable to the so-called, needle-shape GP-II zones [6], pre-β'' phase [24] or β'' phase [1,2,5,6] in wrought alloys. It should be noted that the pre-β'' phase was considered as the most developed GP zones containing Al as a constituent and its formula was written as $(Al+Mg)_5Si_6$ [24]. The phase giving peak strength was usually reported as β' for cast alloys, e.g. [22]. Disagreement was observed in the present work for which peak strength was in association with the β'' phase or its precursors, as reported for wrought alloy, e.g. [9,11,25].

At the beginning of the T6 over-ageing period, a comparatively large, rod-shape phase was formed, as shown in Figure 8(a), at the expense of the needle-shaped phase described above. Its corresponding SADP, separated from that of the Al matrix in Figure 8(b), can be indexed as hexagonal β'. Prolonged over-ageing caused disappearance of the fine, needle-shape phase and growth of fcc $\beta(Mg_2Si)$ frequently with a twin formation in its structure as shown in Figure 8(c) and 8(d).

TEM investigation of the samples after T6I6 ageing revealed comparable micro-structure, except that a higher number density was observed for the needle-shape GP phase at the peak ageing condition. This could result from promotion of secondary precipitation of precursors to the β'' phase [12].

4. CONCLUSIONS

An experimental alloy with a chemical composition equivalent to cast A356 Al-Mg-

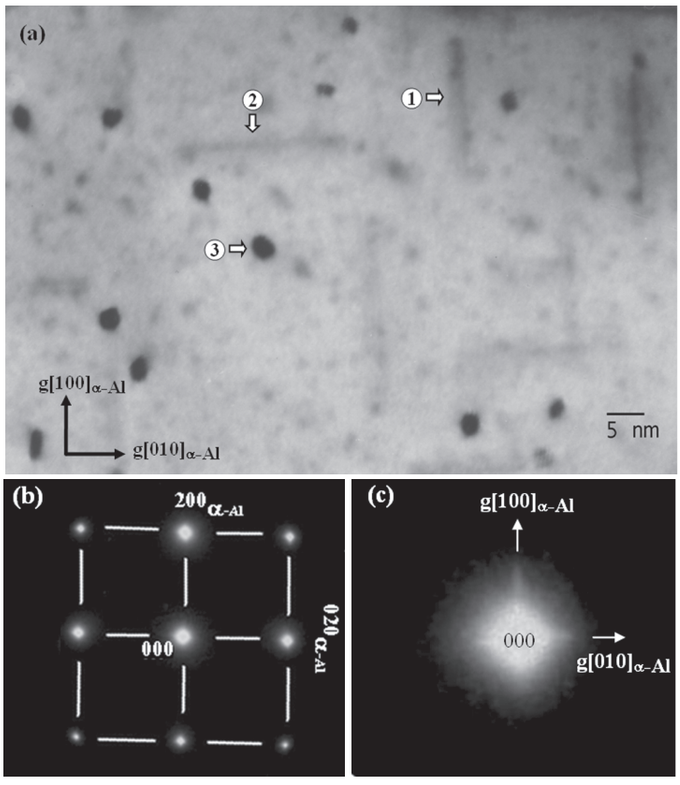

Figure 7. (a) TEM-BF micrograph shows a needle-shaped phase in association with peak strength period of T6 ageing for 24 hours. (b) and (c) are corresponding SADP and the enlargement of the 020 spot revealing streaking along $g<001>_{\alpha\text{-Al}}$.

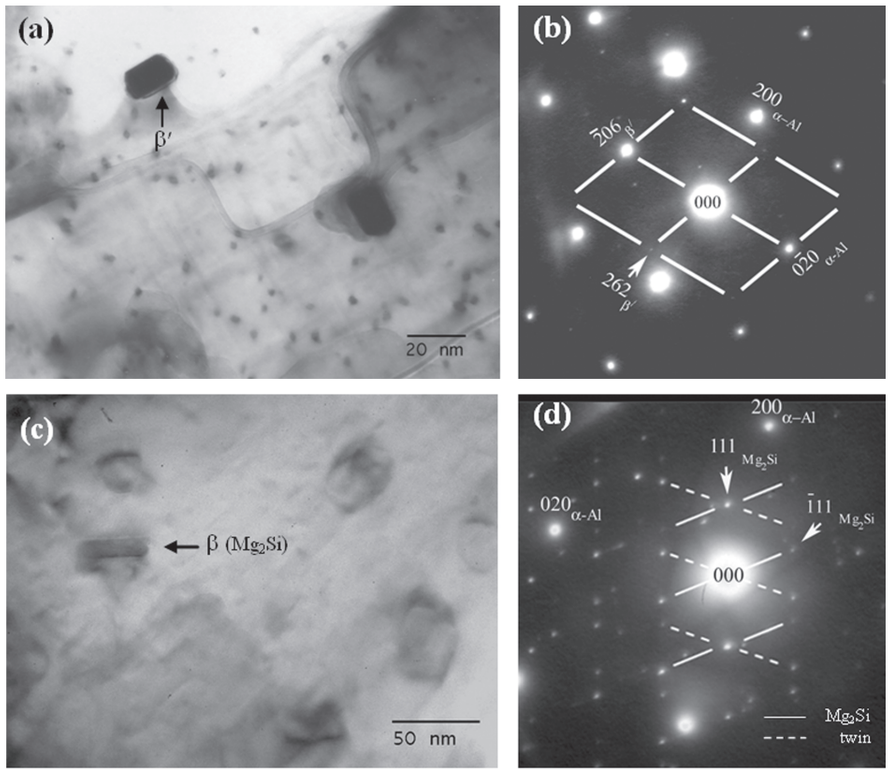

Figure 8. TEM-BF micrographs show precipitated phases in association with T6 over-ageing period; (a) 100 hours, (c) 300 hours. (b) and (d) are corresponding SADPs from β(Mg_2Si) particles indicated by the arrows in (a) and (c), respectively.

Si alloy has been studied. After solution treatment and natural ageing at room temperature, T6 and T6I6 artificial ageing were performed. For both T6 and T6I6, the peak hardness level during ageing was reached after about 24 hours. Ageing hardening by T6 and T6I6 in this experiment increased the Vickers microhardness from the as-cast value by 52% and 60%, respectively. The peak hardness by T6I6 is approximately 8% higher than that obtained by T6. The rate of decrease in hardness from the peak hardness in the over-ageing period was faster in the case of T6I6. SEM revealed eutectic constituents as Si flakes and Fe-bearing intermetallic compounds including p-Chinese script phase ($Al_8Mg_3FeSi_6$) and b(Al_5FeSi). TEM suggested similar precipitation sequence for both T6 and T6I6 as reported previously for wrought and cast Al-Mg-Si alloy. However, the peak ageing period was in association with the β′′ phase or its precursors, not the β′ phase.

ACKNOWLEDGEMENTS

The authors would like to thank the Electron Microscopy Research and Service Center (EMRSc), Faculty of Science, Chiang Mai University, for electron microscopy facilities. The Thailand Graduate Institute of Science and Technology (TGIST) is thanked for a scholarship of S. Imurai.

REFERENCES

[1] Burger G.B., Gupta A.K., Jeffrey P.W.

and Lloyd D.J., Microstructural control of aluminum sheet used in automotive applications, *Mater. Charact*., 1995; **35**: 23-39.

[2] Edward G.A., Stiller K., Dunlop G.L. and Couper M.J., The precipitation sequence in Al-Mg-Si alloys, *Acta mater*., 1998; **46**: 3893-3904.

[3] Maruyama N., Uemori R., Hashimoto N., Saga M. and Kikuchi M., Effect of silicon addition on the composition and structure of fine-scsle precipitates in Al-Mg-Si alloys, *Scripta mater.,* 1997; **36:1**: 89-93.

[4] Gupta A.K., Lloyd D.J. and Court S.A., Precipitation hardening in Al-Mg-Si alloys with and without excess Si, *Mater. Sci. Eng,* 2001**; A316**: 11-17.

[5] Andersen S.J., Zandbergen H.W., Jansen J., Treholt C., Tundal U. and Reiso O., The Crystal Structure of the β" Phase in Al-Mg-Si alloys, *Acta mater.,* 1998; 46:9: 3283-3298.

[6] Dutta I. and Allen S.M., A calorimetric study of precipitation in commercial aluminium alloy 6061, *J. Mater. Sci. Lett.,* 1991; **10**: 323.

[7] Sagalowicz L., Lapasset G. and Hug G., Transmission electron microscopy study of a precipitate which forms in the Al-Mg-Si system, *Phil. Mag. Lett.,* 1996; 74:2: 57-66.

[8] Perovic A., Perovic D.D., Weaterly G.C. and Lloyd D.J., Precipitation in aluminum alloys aa6111 and AA6016, *Scripta Mater.,* 1999; **41:7**: 703-708.

[9] Gupta A.K., Lloyd D.J. and Court S.A., Precipitation hardening processes in an Al-0.4%Mg-1.3%Si-0.25%Fe aluminum alloy, *Mater. Sci. Eng.,* 2001; **A301**: 140-146.

[10] Matsuda K., Sakaguchi Y., Miyata Y., Uetani Y., Sato T., Kamio A. and Ikeno S., Pricipitation sequence of various kinds of metastable phases in Al-1.0mass% Mg_2Si-0.4mass% Si alloy, *J. Mater. Sci*., 2000; **35**: 179-189.

[11] Miao W.F. and Laughlin D.E., Precipitation hardening in aluminium alloy 6022, *Scripta Mater*., 1999; **40**: 873-878.

[12] Buha J., Lumley R.N., Crosky A.G. and Hono K., Secondary precipitation in an Al-Mg-Si-Cu alloy, *Acta Mater*., 2007; **55**: 3015-3024.

[13] Cayron C. and Buffat P.A., Transmission electron microscopy study of the □' phase (Al-Mg-Si alloys) and QC phase (Al-Cu-Mg-Si alloys):ordering mechanism and crystallographic structure, *Acta Mater*., 2000; **48**: 2639-2653.

[14] Caton M.J., Jones J.W., Boileau J.M. and Allison J.E., The effect of solidification rate on the growth of small fatigue cracks in a cast 319-type aliminium alloy, *Metall. Mater. Trans. A.,* 1999; **30A**: 3055.

[15] Miller W.S., Zhuang L., Bottema J., Wittebrood A.J., De Smet P., Haszler A. and Vieregge A., Recent development in aluminium alloys for the Automotive industry, *Mater. Sci. Eng.,* 2000; **A280**: 37-49.

[16] Wang Q.G., Microstructural effects on the tensile and fracture behavior of aluminum casting alloys A356/357, *Metall. Mater. Trans.,* 2003; **34A**: 2887-2896.

[17] Es-Said O.S., Lee D., Pfost W.D., Thompson D.L., Patterson M., Foyos J. and Marloth R., Alternative heat treatments for A357-T6 aluminum alloy, *Eng. Fail. Anal.,* 2002; **9**: 99-107.

[18] Meyers C.W., Solution heat treatment effects on ultimate tensile strength and uniform elongation in A357 aluminum alloys, *AFS Transactions*, 1986; **91**: 511-518.

[19] Apelian D., Shivkumar S. and Sigworth G., Fundamental aspects of heat

treatment of cast Al-Si-Mg alloys, *AFS Transactions*, 1989; **137**: 727-742.

[20] Shivkumar S., Ricci S., Steenhoff Jr. B., Apelian D., and Sigworth G., An experimental study to optimize the heat treatment of A356 alloy, *AFS Transactions*, 1989; **138**: 791-810.

[21] Wang Q.G., Plastic deformation behavior of aluminum casting alloys A356/357, *Metall. Mater. Trans.,* 2004; **35A**: 2707-2718.

[22] Ran G., Zhou J. and Wang Q.G., The effect of hot isoostatic pressing on the microstructure and tensil properties of an unmodified A356-T6 cast aluminum alloy, *J. Alloy Compd.,* 2006; **421**: 80-86.

[23] Mariora C.D., Andersen S.J., Jansen J. and Zandbergen H. W., Atomic model for GP-zone in A 6082 Al-Mg-Si system, *Acta mater.*, 2001; **49**: 321-328.

[24] Cai M., Field D.P. and Lorimer G.W., A systematic comparison of ststic and dynamic ageing of two Al-Mg-Si alloya, *Mater. Sci. Eng.,* 2004; **A373**: 65.

[25] Joint Committee on Powder Diffraction Standards (JCPDS) Files No. 34-0458.